Published in final edited form as:
J Bone Miner Res. 2013 March ; 28(3): 586–597. doi:10.1002/jbmr.1765.

PTH Enhanced Structural Allograft Healing is Associated with Decreased Angiopoietin-2 Mediated Arteriogenesis, Mast Cell Accumulation and Fibrosis

Robinder S. Dhillon[1,2], **Chao Xie**[1,2], **Wakenda Tyler**[1,2], **Laura M. Calvi**[1,3], **Hani A. Awad**[1,4], **Michael J. Zuscik**[1,2], **Regis J. O'Keefe**[1,2], and **Edward M. Schwarz**[1,2,3,4,*]

[1]The Center for Musculoskeletal Research, University of Rochester, Rochester, NY 14642, USA

[2]Department of Orthopaedics, University of Rochester, Rochester, NY 14642, USA

[3]Department of Medicine, University of Rochester, Rochester, NY 14642, USA

[4]Department of Biomedical Engineering, University of Rochester, Rochester, NY 14642, USA

Abstract

Recombinant parathyroid hormone (rPTH) therapy has been evaluated for skeletal repair in animal studies and clinical trials based on its known anabolic effects, but its effects on angiogenesis and fibrosis remain poorly understood. We examined the effects of rPTH therapy on blood vessel formation and osseous integration in a murine femoral allograft model, which caused a significant increase in small vessel numbers, and decreased large vessel formation ($p < 0.05$). Histology showed that rPTH also reduced fibrosis around the allografts to similar levels observed in live autografts, and decreased mast cells at the graft-host junction. Similar effects on vasculogenesis and fibrosis were observed in femoral allografts from Col1caPTHR transgenic mice. Gene expression profiling revealed rPTH induced *angiopoietin-1* (8-fold), while decreasing *angiopoietin-2* (70-fold) at day 7 of allograft healing. Finally, we demonstrate anti-angiopoietin-2 peptibody(L1-10) treatment mimics rPTH effects on angiogenesis and fibrosis. Collectively, these findings demonstrate that intermittent rPTH treatment enhances structural allograft healing by two processes: 1) anabolic effects on new bone formation via small vessel angiogenesis, and 2) inhibition of angiopoietin-2 mediated arteriogenesis. The latter effect may function as a vascular sieve to limit mast cell access to the site of tissue repair, which decreases fibrosis around and between the fractured ends of bone. Thus, rPTH therapy may be generalizable to all forms of tissue repair that suffer from limited biointegration and excessive fibrosis.

Keywords

recombinant parathyroid hormone (rPTH); angiopoietin; arteriogenesis; vasculogenesis; angiogenesis; allograft healing; fibrosis; mast cell

INTRODUCTION

The clinical management of critical (>3cm) segmental defects remains a major challenge for both amputation and limb salvage approaches, which continue to suffer from poor long-term outcomes(1, 2). Although devitalized cortical allografts lack osteogenic potential, they

*To whom correspondence should be addressed: Prof. Edward M. Schwarz, The Center for Musculoskeletal Research, University of Rochester Medical Center, 601 Elmwood Avenue, Box 665, Rochester, NY 14642, Phone: 585-275-3063, Fax: 585-756-4727, edward_schwarz@urmc.rochester.edu.

remain widely used for reconstructive surgery since no synthetic alternatives with comparable biological and biomechanical properties have been developed. Unfortunately, the limited new bone formation and lack of remodeling associated with massive allograft healing are directly associated with the 23–43% clinical failure rate caused by non-union (27–34%), late graft fracture (24–27%), and infection (9–16%)(3). Thus, the development of an adjuvant therapy for patients recovering from reconstructive surgery for critical defects remains a high priority.

Based on its well-known anabolic effects on bone(4–6), recombinant parathyroid hormone (rPTH), either as the full-length ($PTH_{1–84}$) or N-terminal ($PTH_{1–34}$) peptide, has been extensively studied in animal models(7–13) and clinical trials(14–16) of fracture healing with very promising results. We have also observed remarkable rPTH effects in a murine femoral allograft model, in which bone formation only occurs at the graft-host junction due to the host response to the necrotic allograft(17, 18). While the increased bone formation in the rPTH treated allografts was predicted, we were surprised by the remarkable decrease in fibrosis around the allografts, which lead to greater boney union between the graft and the host, and increased biomechanical properties(17, 18). Another unexpected finding was the apparent decrease in the vascularity of rPTH treated allografts (unpublished data), which contrasts data demonstrating that increased angiogenesis from exogenous vascular endothelial growth factor A (VEGF-A) accelerates skeletal repair(19–22). However, recent studies have shown that while rPTH-induced bone formation is VEGF-A dependent, its anabolic effects occur without increasing bone vessel density by redistribution of smaller vessels closer to bone formation sites(13). As elucidating the mechanism of decreased fibrosis has broad implications for all tissue engineering and regenerative medicine applications, we tested the hypothesis that rPTH therapy promotes small vessel angiogenesis and inhibits large vessel arteriogenesis during structural allograft healing in mice. The PTH/PTH-related protein receptor (PPR) has a central role in mediating the diverse actions of PTH on bone in vivo(23). It is evident that intermittent (once daily) exogenous rPTH administration has an anabolic effect on bone(24), whereas the continuous exposure to PTH, as in hyperparathyroidism, leads to hypercalcaemia and a net decrease in bone volume(25), which is referred to as its ‘catabolic effect’. In an attempt to elucidate these differential effects and mechanisms of PTH action in our femoral allograft model, we utilized Col1caPTHR transgenic mice that have a constitutively active PPR receptor under the Col1 promoter(26). These mice have a high trabecular bone mass with increased osteoclast activity due to increased osteoblast numbers and high bone turnover. Since this genetic model of PTH gain of function is specific to osteoblasts, this system allowed us to test if osteoblasts are the primary target of rPTH therapy during allograft healing.

MATERIALS AND METHODS

Femoral Autograft and Allograft Model

All experiments with live animals were performed on University of Rochester Committee for Animal Resources approved protocols. Femoral autograft and allograft surgeries were performed on mice as previously described(20). Briefly, a 4-mm mid-diaphyseal osteotomy was created in the host mouse and then replaced with the same bone (live autograft), or an acellular mid-diaphyseal femoral segment from an allogenic strain.

Experimental Animals

Experiment 1—8 weeks old female C57/BL6 mice underwent live autograft or allograft surgery. The allografted mice were randomized to treatment with daily intraperitoneal injections of teriparatide (40μg/kg/day human $PTH_{1–34}$Forteo™, Eli Lilly and Co., Indianapolis, IN) (n=5) or saline (placebo) (n=5) as previously described(17). Mice were

euthanized on day 7, 10, 14, 21 or 28 post-op for gene expression studies, and additional mice were euthanized on days 21 and 28 for micro-CT and histology.

Experiment 2—8 week old Col1-caPTHR mice(26) (n=5) and their WT littermates (n=5) in a FVB background received allografts or live isografts from Col1-caPTHR mice, and the grafted femurs were harvested after euthanasia on day 21 or 28 post-op for micro-CT and histology analyses.

Experiment 3—8 weeks old female C57/BL6 mice underwent allograft surgery. The allografted mice were randomized to treatment with biweekly intraperitoneal injections of L1-10(27) (3mg/kg/dose) (n=5), a recombinant peptide-Fc fusion protein (peptibody) that selectively inhibits angiopoietin-2 (Ang-2) binding to its tyrosine kinase receptor (Tie2)(28), AMGEN Inc., Thousand Oaks, CA) or saline (placebo) (n=5). Mice were euthanized on day 21 post-op for micro-CT, histology and histomorphometry.

X-rays, Vascular Perfusion and Micro-CT

Longitudinal plain radiographs were obtained using the Faxitron Cabinet X-ray System (Faxitron X-ray, Wheeling, IL, USA) as previously described (20). Animals were then euthanized using lead chromate intra-cardiac infusion as previously described (29). Briefly, the mice were anesthetized and thoracotomy was performed to insert a 20-gauge angiocatheter into the left ventricle. The circulatory system was flushed with 20 ml of 0.9% saline and heparin (100 IU/ml), followed by 20 ml of 10% neutral buffered formalin. This procedure was immediately followed by injection of 4 ml lead base contrast agent MICROFIL MV-122 (Flow Tech, Inc., Carver, MA) via the same route. The femurs were harvested, intramedullary pin removed, and the specimens were stored in 10% neutral buffered formalin until the initial micro-CT scan was performed using a 10.5 micron isotropic high resolution micro-CT (VivaCT 40; Scanco Medical AG, Basserdorf, Switzerland). Following the initial micro-CT scan, the specimens were then decalcified for 4–6 weeks in ethylene, diamine, tetra-acetic acid (EDTA). Following decalcification, the specimens were subjected to second micro-CT scan. Volumetric bone and vascular quantification was performed on the region of interest (ROI), which spanned the 4mm graft and 1mm of the host femur on both the proximal and distal graft junction as previously described(29).

Histology and Pilot Histomorphometry

Following micro-CT, the femurs were dissected and processed for decalcified histology in paraffin as previously described(29). At least three nonconsecutive 4-μm paraffin embedded mid-sagittal sections of the ROI from each specimen were stained with either alcian blue/ hematoxylin/orange G (AB/OG), or for tartrate resistant acid phosphatase (TRAP) and counter stained with safrin-O. Osteoclasts were defined as multinucleated cells (>3 nuclei) TRAP-positive cells on a bone surface in the ROI. Histomorphometry to quantify osteoclast and mast cell numbers, and mesenchymal tissue, cartilage and bone area using Osteometrics Software (Decatur, GA), was performed on 3 parallel section >0.2mm apart from each femur in which the mean values are the data for each mouse (n=5).

Gene Expression Analyses

Grafted femurs were harvested, the 6mm ROI including the 4mm of graft and 1 mm of host at each end was homogenized using TissueLyser II (Qiagen, Hilden, Germany), and total RNA was extracted using the RNeasy mini purification kit (Qiagen, Valencia, CA) according to manufacturer's protocol. The mRNA was reverse-transcribed using an iScript cDNA synthesis kit (Bio-Rad Lab, Hercules, CA) and the cDNA was used as the template

for real-time PCR analyses with the following gene specific primers obtained from Integrated DNA Technologies (IDT, Coralville, IA).

Angiopoietin-1	FORWARD	5'-CCA TGC TTG AGA TAG GAA CCA G-3'
	REVERSE	5'-TTC AAG TCG GGA TGT TTG ATT T-3'
Angiopoietin-2	FORWARD	5'-AGC AGA TTT TGG ATC AGA CCA G-3'
	REVERSE	5'-GCT CCT TCA TGG ACT GTA GCT G-3'
Tie-2	FORWARD	5'-CGG CTT AGT TCT CTG TGG AGT C-3'
	REVERSE	5'-GGC ATC AGA CAC AAG AGG TAG G-3'
β -Actin	FORWARD	5'-AGA TGT GGA TCA GCA AGC AG-3'
	REVERSE	5'-GCG CAA GTT AGG TTT TGT CA-3'

Each reaction was carried out in a final volume of 20 ml consisting of 0.1 mM primers, 1 ml Sybr Green PCR Super Mix (ABgene, Thermo Fisher Scientific Inc, Rochester, NY), and 1 ml of the purified cDNA template. The samples were assayed in triplicate in a Rotor-Gene RG 3000 (Corbett Research, Sydney, AU). Mouse β-actin was used as the reference gene to normalize for differences in the amount of total RNA in each sample. For quantification, the relative level (mean +/− SD) of each group normalized to β-actin was determined as the fold-change vs. Day 7 autograft.

Statistics

Results are shown as the mean value plus or minus the standard deviation (+/−SD) of the mean. All statistical analysis was performed using Prism statistical package Version 4.0 (GraphPad, San Diego, CA) with p values <0.05 being considered statistically significant. A one-way analysis of variance (ANOVA), Newman–Keuls multiple comparison test, *t* test and Mann-Whitney and Spearman's rank correlation coefficient was used for all statistical analyses. Significant differences in bridging new cortical bone formation were determined by Fisher's exact test.

RESULTS

Intermittent rPTH therapy promotes small vessel angiogenesis and inhibits large vessel arteriogenesis during femoral allograft healing

In order to establish the effects of intermittent rPTH treatment on the neovascularization of structural allografts following implantation, we performed a time course experiment in which mice received a femoral allograft surgery and were randomized to daily rPTH or placebo injections. The allografted femurs were harvested on days 7, 10, 14, 21 and 28 following surgery, and analyzed by micro-CT and histology versus a live autograft control group following radiographic confirmation of rPTH anabolic effects on bone formation (Supplemental Figures 1 and 2). The results revealed that rPTH significantly affects allograft vascularity as early as day 14 post-op (Figure 1). At day 28 rPTH significantly decreased total allograft vascularity compared to placebo (vascular volume = 0.58 ± 0.10 compared to 1.06 ± 0.19 mm^3; mean vessel diameter = 0.08 ± 0.01 vs. 0.10 ± 0.01 mm; $p<0.05$). Review of the histology slides revealed a clear phenotypic difference between the sizes of lead-chromate perfused blood vessels, in that the vessels of the rPTH treated allografts appeared to be more abundant and markedly smaller vs. placebo (Figure 1B-1E). At day 28 rPTH significantly decreased total allograft vascularity and the mean vessel diameter compared to placebo (Figure 1F & 1G). Contrary to the gross overall decrease in vascularity as assessed

by micro-CT, pilot histomorphometry clarified this anomaly depicting a marked increase in the vascular parameters in rPTH treated allografts vs. placebo (Table 1).

To further confirm these differences, we quantified the number of smaller vs. larger perfused vessels via micro-CT of allografts harvested on day 21 and 28 (Figure 2), which demonstrates that rPTH treated allografts have significantly more small vessels (<90μm), and significantly fewer large vessels (>90μm) vs. placebo. Interestingly, this alteration in neovascularization corresponded with a dramatic alteration in the fibrotic tissue response versus the chondrogenic and osteogenic response in the placebo vs. rPTH treated allografts respectively. Confirmatory histomorphometry revealed that the tissue composition of rPTH treated allografts is remarkably similar to that of live autografts, in contrast to the fibrosis observed in placebo (Figure 3A-E).

In order to elucidate the mechanism by which PTH signaling decreases large vessel arteriogenesis during allograft healing, we performed gene expression studies on femurs that received live autografts, or allografts followed by daily placebo or rPTH therapy for 7, 10 and 14 days. Although significant ~2-fold increases in *vegf-a* and *vegfr-r2* mRNA levels were detected in the rPTH treated allografts (Supplemental Figure 3), the most remarkable findings revealed a reciprocal regulation of *angiopoietin* (*ang*) genes on day 7. We observed an 8-fold increase in ang-1, and a 35-fold decrease of ang-2 mRNA levels in healing allografts from rPTH treated mice vs. placebo (Figure 3F-G). Since Ang-2 is known to be critically involved in remodeling small capillaries into large vascular networks and Ang-1 is a known Ang-2 antagonist (30, 31), this novel finding suggests that rPTH inhibits large vessel arteriogenesis during allograft healing via reciprocal regulation of these factors.

Constitutive PTHR signaling in osteoblastic cells promotes small vessel angiogenesis and inhibits large vessel arteriogenesis during femoral allograft healing and extensive graft resorption

In order to confirm our observations on allograft vascularity, and further define the target cells of rPTH treatment in our model, we repeated the femoral allograft experiment using Col1-caPTHR transgenic mice and their non-transgenic littermates as controls. The micro-CT and histology results from these experiments were remarkably similar to that of the rPTH vs. placebo treatments (Figure 4). Specifically, micro-CT analyses displayed a similar decrease in vascularity of the allografts in Col1-caPTHR mice compared to their WT littermates on day 28 (vascular volume 0.36 ± 0.09 vs.1.01 ± 0.31 mm^3; vessel number 1.01 ± 0.11 vs.1.26 ± 0.06 mm; $p<0.05$), and histology (Figure 4B-E) revealed the same small vs. large vessel ratio that was seen in placebo versus rPTH-treated mice. However, there were two remarkable differences between rPTH and Col1-caPTHR which could be attributed to intermittent vs. continuous PTH signaling. The first is that both large and small blood vessel formation in Col1-caPTHR allografts are suppressed at 21 days, as the significant increase in small vessel numbers (≤90μm) vs. WT did not occur until day 28 (Figure 5). The other major dissimilarity is that while we did not observe any significant differences between allograft bone volume and osteoclast numbers in rPTH vs. placebo treated allografts (data not shown), x-rays revealed that femoral allografts in Col1-caPTHR mice are rapidly resorbed (Supplemental Figure 4) due to a significant increase in osteoclast numbers (Table 2).

Intermittent rPTH treatment reduces mast cell numbers in healing allografts

Upon scrutiny of toluidine blue stained histology sections to assess cartilage formation during allograft healing, we notice a paucity of mast cells (Supplemental Figure 6) in immediate proximity to blood vessels in the transitional tissue adjacent to the allografts of rPTH treated mice compared to placebo (Figure 6A-F). Pilot histomorphometry showed that

there appears to be a 2-fold decrease in mast cell numbers at the allograft-host junction on day 21 in rPTH vs. placebo treated mice, while no differences in mast cell numbers in the adjacent skeletal muscle were observed (Table 3).

Anti-Ang-2 treatment mimics rPTH effects on arteriogenesis, fibrosis and mast cell recruitment during allograft healing

To test the functional importance of angiopoietin-2 during structural allograft healing, we performed femoral allograft surgery on mice randomized to placebo or (L1-10), a recombinant peptide-Fc fusion protein (peptibody) that selectively inhibits angiopoietin-2 (Ang-2) binding to its tyrosine kinase receptor (Tie2), and harvested the grafted femurs on day 21 for micro-CT analyses. As expected, anti-Ang2 (L1-10) therapy had no effect on small vessel formation, but significantly inhibited the formation of perfused vessels >180μm in diameter (Figure 7A). We also performed histology analyses on these samples and confirmed that anti-Ang2 treatment mimics PTH treatment in decreasing fibrosis, mast cell accumulation and arteriogenesis during allograft healing (Figure 7B). Furthermore, we observed a significant increase in host-to-host bony union (5 out of 5 anti-Ang2 vs. 0 out of 5 placebo; $p<0.05$ by Fisher's Exact Test), evidence by the presence of new bone that formed along the allograft surface (Figure 7C). Since these outcome measures closely correlate with biomechanical healing of structural allografts(32), it suggests that inhibition of arteriogenesis, mast cell infiltration and fibrosis via anti-Ang2 treatment may be an effective adjuvant therapy following tissue reconstruction.

DISCUSSION

Despite the remarkable advances in reconstructive surgery and musculoskeletal tissue engineering to correct segmental defects over the last two decades, effective healing between the host and the implant remains a major challenge due to fibrosis at the interface. In the case of bone healing, which occurs through a highly regulated temporal process that proceeds from an initial inflammatory phase(33), blood and periosteum derived mesenchymal stem cells (MSC) at the fracture site must respond to biological and biomechanical cues to appropriately differentiate into chondrocytes and osteoblasts that will produce the bridging matrix. When this process is challenged by disease, infection, drugs, aging or excessive tissue damage, MSC differentiation can be diverted to fibroblastic cells, leading to fibrosis at the interface and non-union. To better understand the etiology of fibrosis we examined the effects of rPTH therapy on blood vessel formation and osseous integration during femoral allograft healing. The results demonstrated that rPTH causes a significant increase in small vessel numbers, and decreased large vessel formation (Table 1; Figures 1 and 2). Moreover, rPTH appeared to markedly reduced fibrosis around the allografts to levels observed in live autografts (Figure 3), and decreased mast cell numbers at the graft-host junction (Table 3; Figure 6). As these rPTH affects on allograft healing were recapitulated by femoral allografts in Col1caPTHR mice (Table 2; Figures 4 and 5), our findings suggest that rPTH exerts its effects directly on osteoblasts at the site of bone repair. At the molecular level, our findings that rPTH reciprocally regulates *angiopoietin-1* and *angiopoietin-2* at day 7 of allograft healing (Figure 3), and that anti-angiopoietin-2 peptibody(L1-10) treatment mimics rPTH effects on angiogenesis and fibrosis (Figure 7), suggests that decreasing Ang-2 mediated arteriogenesis is a critical mechanism of action of rPTH therapy for bone repair. Given that the decreased arteriogenesis and fibrosis is associated with decreased mast cell numbers, it is tempting to speculating that the rPTH effects on angiogenesis function as a vascular sieve to limit pro-fibrotic cell access to the site of tissue repair to allow tissue repair without scaring, and future studies to directly test this hypothesis are warranted.

While angiogenesis is known to be a critical process during fracture repair (34), the nature of these new vessel (small capillaries vs. large vessels) and their proximity to newly forming bone has only recently been investigated(13). Gene expression studies in animal models have demonstrated that angiogenic factors (*Vegf-a, neuropilin, Ang, Vegfr-2, Tie-2* and *Hif-1a*) are immediately induced following fracture(35, 36), which is consistent with the known roles of angiogenesis in MSC recruitment, vascular invasion of the hypertrophy cartilage and calcification of the soft callus, and intramembranous bone formation. However, it is also known that vascular regression is required for mesenchymal condensation and chondrogenesis, and that disruption of this hypoxic environment via VEGF-induced angiogenesis leads to decreased cartilage formation(37). Thus, our observation that rPTH limits the magnitude of vasculogenesis following structural allograft healing, to mimic that observed in the chondrogenic stages of autograft healing (Figure 1 & 3), provides additional insight as to how this therapy stimulates cartilage formation vs. fibrosis at the graft-host junction.

It has long been recognized that mast cells may play an important role in fracture healing(38). Histology studies of fractures in a rat model revealed that in the first two weeks, mast cells are found either in the vicinity of blood vessels or in the vascularized tissue proliferating into the cartilaginous portion of subperiosteal callus(39). This finding led to the view that mast cells are involved in digestion of extracellular matrix and angiogenesis in the early stages of fracture healing. However, mast cells are also known to be central mediators of chronic fibrosis via degranulation and release of fibroblast growth factors, TGFβ and other factors that promote progressive sclerosis(40). Thus, our finding that rPTH therapy markedly decreases mast cell numbers in the transitional tissue between healing structural allografts and the adjacent skeletal muscle (Figure 5) suggests another potential anti-fibrotic mechanism of this intervention. While it is attractive for us to speculate that the decrease in mast cell numbers is related to the decreased large vessel formation in rPTH treated allografts, future studies are needed to formally establish this relationship.

In order to identify the direct mechanism of rPTH decreased arteriogenesis during allograft healing we perform a broad gene expression analysis of angiogenic factors, which focused our attention on *Angiopoietins* (data not shown). Our finding that *Ang-2* is expressed 70-fold higher in allografts vs. autografts on day 7, and that rPTH therapy reduces this expression level in allografts down to that observed in autografts, strongly implicates Ang-2 as a dominant mediator of arteriogenesis in our model (Figure 3f & 3g). Interestingly, this rPTH-mediated decreased *Ang-2* expression occurred with a reciprocal 8-fold increase in *Ang-1* levels, which is somewhat surprising considering that Ang-1 is pro-angiogenic(41–43). However, it is noteworthy that other studies have shown that Ang-1 inhibits angiogenesis, and vascular permeability(44–48). Thus, this rPTH-induced reciprocal regulation of Ang-1 and Ang-2 could be an important factor in the decreased vasculogenesis. More importantly, the demonstration that anti-Ang2 therapy selectively and significantly inhibits large vessel (>0.18mm) formation during allograft healing (Figure 6a), and significantly enhances bony union by decreasing the amount of fibrosis and accelerating *osteogenesis* and *chondrogenesis* (Figure 6b), confirms that Ang-2 is necessary and sufficient for arteriogenesis and fibrosis at the host-allograft interface in this model. As a major clinical indication of structural allografting is reconstruction following bone tumor resection, and rPTH therapy is contraindicated in these patients, our finding that anti-Ang2 therapy achieves a similar outcome has obvious implications for this major unmet need for limb salvage in cancer patients. Additionally, although this research has focused on bone healing, the problem of postoperative fibrosis is common to all surgical procedures. Thus, future studies to evaluate the role of Ang-2 and the effects of rPTH treatment during soft tissue repair and regeneration are warranted.

Supplementary Material

Refer to Web version on PubMed Central for supplementary material.

Acknowledgments

The authors would like to thank AMGEN Inc. for their gift of the *L1-10* peptibody, Ryan Tierney and Sarah Mack for their assistance with the histology and Michael Thullen for technical assistance with micro-CT analyses. This work was supported by research grants from the National Institutes of Health (DE019902, AR054041 and AR061307).

Authors' roles: Study design: ES, RD, LC, WT, RO, HA and CX. Study conduct: RD and CX. Data collection: RD. Data analysis: RD, CX, LC, HA & ES. Data interpretation: ES, RD, LC, WT, RO, HA and CX. Drafting manuscript: ES and RD. Revising manuscript content: ES, CX, LC, MZ, HA and RO. Approving final version of manuscript: RD, CX, WT, LC, HA, MZ, RO and ES. RD & ES takes responsibility for the integrity of the data analysis.

REFERENCES

1. Busse JW, Jacobs CL, Swiontkowski MF, Bosse MJ, Bhandari M. Complex limb salvage or early amputation for severe lower-limb injury: a meta-analysis of observational studies. J Orthop Trauma. 2007 Jan; 21(1):70–76. [PubMed: 17211275]
2. Bosse MJ, MacKenzie EJ, Kellam JF, Burgess AR, Webb LX, Swiontkowski MF, Sanders RW, Jones AL, McAndrew MP, Patterson BM, McCarthy ML, Travison TG, Castillo RC. An analysis of outcomes of reconstruction or amputation after leg-threatening injuries. N Engl J Med. 2002 Dec 12; 347(24):1924–1931. [PubMed: 12477942]
3. Wheeler DL, Enneking WF. Allograft bone decreases in strength in vivo over time. Clin Orthop Relat Res. 2005 Jun.(435):36–42. [PubMed: 15930919]
4. Bukata SV, Puzas JE. Orthopedic uses of teriparatide. Curr Osteoporos Rep. 2010 Mar; 8(1):28–33. [Review]. [PubMed: 20425088]
5. Rubery PT, Bukata SV. Teriparatide may accelerate healing in delayed unions of type III odontoid fractures: a report of 3 cases. J Spinal Disord Tech. 2010 Apr; 23(2):151–155. [Case Reports]. [PubMed: 20051918]
6. Neer RM, Arnaud CD, Zanchetta JR, Prince R, Gaich GA, Reginster JY, Hodsman AB, Eriksen EF, Ish-Shalom S, Genant HK, Wang O, Mitlak BH. Effect of parathyroid hormone (1-34) on fractures and bone mineral density in postmenopausal women with osteoporosis. N Engl J Med. 2001 May 10; 344(19):1434–1441. [Clinical Trial Multicenter Study Randomized Controlled Trial Research Support, Non-U.S Gov't]. [PubMed: 11346808]
7. Komatsubara S, Mori S, Mashiba T, Nonaka K, Seki A, Akiyama T, Miyamoto K, Cao Y, Manabe T, Norimatsu H. Human parathyroid hormone (1-34) accelerates the fracture healing process of woven to lamellar bone replacement and new cortical shell formation in rat femora. Bone. 2005 Apr; 36(4):678–687. [PubMed: 15781006]
8. Andreassen TT, Ejersted C, Oxlund H. Intermittent parathyroid hormone (1-34) treatment increases callus formation and mechanical strength of healing rat fractures. J Bone Miner Res. 1999 Jun; 14(6):960–968. [PubMed: 10352105]
9. Andreassen TT, Willick GE, Morley P, Whitfield JF. Treatment with parathyroid hormone hPTH(1-34), hPTH(1-31), and monocyclic hPTH(1-31) enhances fracture strength and callus amount after withdrawal fracture strength and callus mechanical quality continue to increase. Calcif Tissue Int. 2004 Apr; 74(4):351–356. [PubMed: 15255072]
10. Andreassen TT, Fledelius C, Ejersted C, Oxlund H. Increases in callus formation and mechanical strength of healing fractures in old rats treated with parathyroid hormone. Acta Orthop Scand. 2001 Jun; 72(3):304–307. [PubMed: 11480610]
11. Nakazawa T, Nakajima A, Shiomi K, Moriya H, Einhorn TA, Yamazaki M. Effects of low-dose, intermittent treatment with recombinant human parathyroid hormone (1-34) on chondrogenesis in a model of experimental fracture healing. Bone. 2005 Nov; 37(5):711–719. [PubMed: 16143574]

12. Nakajima A, Shimoji N, Shiomi K, Shimizu S, Moriya H, Einhorn TA, Yamazaki M. Mechanisms for the enhancement of fracture healing in rats treated with intermittent low-dose human parathyroid hormone (1-34). J Bone Miner Res. 2002 Nov; 17(11):2038–2047. [PubMed: 12412812]

13. Prisby R, Guignandon A, Vanden-Bossche A, Mac-Way F, Linossier MT, Thomas M, Laroche N, Malaval L, Langer M, Peter ZA, Peyrin F, Vico L, Lafage-Proust MH. Intermittent PTH(1-84) is osteoanabolic but not osteoangiogenic and relocates bone marrow blood vessels closer to bone-forming sites. J Bone Miner Res. 2011 Nov; 26(11):2583–2596. [PubMed: 21713994]

14. Aspenberg P, Genant HK, Johansson T, Nino AJ, See K, Krohn K, Garcia-Hernandez PA, Recknor CP, Einhorn TA, Dalsky GP, Mitlak BH, Fierlinger A, Lakshmanan MC. Teriparatide for Acceleration of Fracture Repair in Humans: A Prospective, Randomized, Double-blind Study of 102 Postmenopausal Women with Distal Radial Fractures. J Bone Miner Res. 2009 Jul 13.

15. Aspenberg P, Johansson T. Teriparatide improves early callus formation in distal radial fractures. Acta Orthop. 2010 Apr; 81(2):234–236. [PubMed: 20367417]

16. Peichl P, Holzer LA, Maier R, Holzer G. Parathyroid hormone 1-84 accelerates fracture-healing in pubic bones of elderly osteoporotic women. J Bone Joint Surg Am. 2011 Sep 7; 93(17):1583–1587. [PubMed: 21915572]

17. Reynolds DG, Takahata M, Lerner AL, O'Keefe RJ, Schwarz EM, Awad HA. Teriparatide therapy enhances devitalized femoral allograft osseointegration and biomechanics in a murine model. Bone. 2010 Mar 1; 48(3):562–570. [PubMed: 20950720]

18. Takahata M, Schwarz EM, Chen T, O'Keefe RJ, Awad HA. Delayed Short Course Treatment with Teriparatide (PTH1-34) Improves Femoral Allograft Healing by Enhancing Intramembranous Bone Formation at the Graft-Host Junction. J Bone Miner Res. 2011 submitted.

19. Peng H, Wright V, Usas A, Gearhart B, Shen HC, Cummins J, Huard J. Synergistic enhancement of bone formation and healing by stem cell-expressed VEGF and bone morphogenetic protein-4. J Clin Invest. 2002 Sep; 110(6):751–759. [PubMed: 12235106]

20. Ito H, Koefoed M, Tiyapatanaputi P, Gromov K, Goater JJ, Carmouche J, Zhang X, Rubery PT, Rabinowitz J, Samulski RJ, Nakamura T, Soballe K, O'Keefe RJ, Boyce BF, Schwarz EM. Remodeling of cortical bone allografts mediated by adherent rAAV-RANKL and VEGF gene therapy. Nat Med. 2005 Mar; 11(3):291–297. [PubMed: 15711561]

21. Kaigler D, Wang Z, Horger K, Mooney DJ, Krebsbach PH. VEGF scaffolds enhance angiogenesis and bone regeneration in irradiated osseous defects. J Bone Miner Res. 2006 May; 21(5):735–744. [PubMed: 16734388]

22. Wan C, Gilbert SR, Wang Y, Cao X, Shen X, Ramaswamy G, Jacobsen KA, Alaql ZS, Eberhardt AW, Gerstenfeld LC, Einhorn TA, Deng L, Clemens TL. Activation of the hypoxia-inducible factor-1alpha pathway accelerates bone regeneration. Proc Natl Acad Sci U S A. 2008 Jan 15; 105(2):686–691. [PubMed: 18184809]

23. Lanske B, Karaplis AC, Lee K, Luz A, Vortkamp A, Pirro A, Karperien M, Defize LH, Ho C, Mulligan RC, Abou-Samra AB, Juppner H, Segre GV, Kronenberg HM. PTH/PTHrP receptor in early development and Indian hedgehog-regulated bone growth. Science. 1996 Aug 2; 273(5275): 663–666. [Research Support, Non-U.S. Gov't Research Support, U.S. Gov't, P.H.S.]. [PubMed: 8662561]

24. Jilka RL. Molecular and cellular mechanisms of the anabolic effect of intermittent PTH. Bone. 2007 Jun; 40(6):1434–1446. [Research Support, N.I.H., Extramural Research Support, U.S. Gov't, Non-P.H.S. Review]. [PubMed: 17517365]

25. Uzawa T, Hori M, Ejiri S, Ozawa H. Comparison of the effects of intermittent and continuous administration of human parathyroid hormone(1-34) on rat bone. Bone. 1995 Apr; 16(4):477–484. [Comparative Study]. [PubMed: 7605709]

26. Calvi LM, Sims NA, Hunzelman JL, Knight MC, Giovannetti A, Saxton JM, Kronenberg HM, Baron R, Schipani E. Activated parathyroid hormone/parathyroid hormone-related protein receptor in osteoblastic cells differentially affects cortical and trabecular bone. J Clin Invest. 2001 Feb; 107(3):277–286. [PubMed: 11160151]

27. Yan ZX, Jiang ZH, Liu NF. Angiopoietin-2 promotes inflammatory lymphangiogenesis and its effect can be blocked by the specific inhibitor L1-10. American journal of physiology Heart and

circulatory physiology. 2012 Jan; 302(1):H215–H223. [Research Support, Non-U.S Gov't]. [PubMed: 22058148]

28. Oliner J, Min H, Leal J, Yu D, Rao S, You E, Tang X, Kim H, Meyer S, Han SJ, Hawkins N, Rosenfeld R, Davy E, Graham K, Jacobsen F, Stevenson S, Ho J, Chen Q, Hartmann T, Michaels M, Kelley M, Li L, Sitney K, Martin F, Sun JR, Zhang N, Lu J, Estrada J, Kumar R, Coxon A, Kaufman S, Pretorius J, Scully S, Cattley R, Payton M, Coats S, Nguyen L, Desilva B, Ndifor A, Hayward I, Radinsky R, Boone T, Kendall R. Suppression of angiogenesis and tumor growth by selective inhibition of angiopoietin-2. Cancer cell. 2004 Nov; 6(5):507–516. [PubMed: 15542434]
29. Zhang X, Xie C, Lin AS, Ito H, Awad H, Lieberman JR, Rubery PT, Schwarz EM, O'Keefe RJ, Guldberg RE. Periosteal progenitor cell fate in segmental cortical bone graft transplantations: implications for functional tissue engineering. J Bone Miner Res. 2005 Dec; 20(12):2124–2137. [Research Support, N.I.H., Extramural Research Support, Non-U.S. Gov't Research Support, U.S. Gov't, Non-P.H.S.]. [PubMed: 16294266]
30. Ahmad SA, Liu W, Jung YD, Fan F, Reinmuth N, Bucana CD, Ellis LM. Differential expression of angiopoietin-1 and angiopoietin-2 in colon carcinoma. A possible mechanism for the initiation of angiogenesis. Cancer. 2001 Sep 1; 92(5):1138–1143. [PubMed: 11571726]
31. Udani V, Santarelli J, Yung Y, Cheshier S, Andrews A, Kasad Z, Tse V. Differential expression of angiopoietin-1 and angiopoietin-2 may enhance recruitment of bone-marrow-derived endothelial precursor cells into brain tumors. Neurol Res. 2005 Dec; 27(8):801–806. [PubMed: 16354539]
32. Reynolds DG, Shaikh S, Papuga MO, Lerner AL, O'Keefe RJ, Schwarz EM, Awad HA. muCT-based measurement of cortical bone graft-to-host union. J Bone Miner Res. 2009 May; 24(5):899–907. [PubMed: 19063685]
33. Einhorn TA. The cell and molecular biology of fracture healing. Clin Orthop. 1998 Oct.(355 Suppl):S7–21. [PubMed: 9917622]
34. Glowacki J. Angiogenesis in fracture repair. Clin Orthop Relat Res. 1998 Oct.(355 Suppl):S82–S89. [PubMed: 9917629]
35. Pacicca DM, Patel N, Lee C, Salisbury K, Lehmann W, Carvalho R, Gerstenfeld LC, Einhorn TA. Expression of angiogenic factors during distraction osteogenesis. Bone. 2003 Dec; 33(6):889–898. [PubMed: 14678848]
36. Carvalho RS, Einhorn TA, Lehmann W, Edgar C, Al-Yamani A, Apazidis A, Pacicca D, Clemens TL, Gerstenfeld LC. The role of angiogenesis in a murine tibial model of distraction osteogenesis. Bone. 2004 May; 34(5):849–861. [PubMed: 15121017]
37. Yin M, Pacifici M. Vascular regression is required for mesenchymal condensation and chondrogenesis in the developing limb. Dev Dyn. 2001 Nov; 222(3):522–533. [PubMed: 11747085]
38. Lindholm R, Lindholm S, Liukko P. Fracture healing and mast cells. I. The periosteal callus in rats. Acta Orthop Scand. 1967; 38(2):115–122. [PubMed: 4166390]
39. Banovac K, Renfree K, Makowski AL, Latta LL, Altman RD. Fracture healing and mast cells. J Orthop Trauma. 1995; 9(6):482–490. [PubMed: 8592261]
40. Puxeddu I, Piliponsky AM, Bachelet I, Levi-Schaffer F. Mast cells in allergy and beyond. Int J Biochem Cell Biol. 2003 Dec; 35(12):1601–1607. [PubMed: 12962699]
41. Hansbury MJ, Nicosia RF, Zhu WH, Holmes SJ, Winkler JD. Production and characterization of a Tie2 agonist monoclonal antibody. Angiogenesis. 2001; 4(1):29–36. [Research Support, U.S. Gov't, P.H.S.]. [PubMed: 11824375]
42. Suri C, McClain J, Thurston G, McDonald DM, Zhou H, Oldmixon EH, Sato TN, Yancopoulos GD. Increased vascularization in mice overexpressing angiopoietin-1. Science. 1998 Oct 16; 282(5388):468–471. [Research Support, U.S. Gov't, P.H.S.]. [PubMed: 9774272]
43. Shim WS, Teh M, Mack PO, Ge R. Inhibition of angiopoietin-1 expression in tumor cells by an antisense RNA approach inhibited xenograft tumor growth in immunodeficient mice. Int J Cancer. 2001 Oct 1; 94(1):6–15. [Research Support, Non-U.S. Gov't]. [PubMed: 11668472]
44. Chae JK, Kim I, Lim ST, Chung MJ, Kim WH, Kim HG, Ko JK, Koh GY. Coadministration of angiopoietin-1 and vascular endothelial growth factor enhances collateral vascularization. Arterioscler Thromb Vasc Biol. 2000 Dec; 20(12):2573–2578. [Comparative Study Research Support, Non-U.S. Gov't]. [PubMed: 11116055]

45. Hayes AJ, Huang WQ, Yu J, Maisonpierre PC, Liu A, Kern FG, Lippman ME, McLeskey SW, Li LY. Expression and function of angiopoietin-1 in breast cancer. Br J Cancer. 2000 Nov; 83(9): 1154–1160. [Research Support, U.S. Gov't, Non-P.H.S.]. [PubMed: 11027428]

46. Stoeltzing O, Ahmad SA, Liu W, McCarty MF, Wey JS, Parikh AA, Fan F, Reinmuth N, Kawaguchi M, Bucana CD, Ellis LM. Angiopoietin-1 inhibits vascular permeability, angiogenesis, and growth of hepatic colon cancer tumors. Cancer Res. 2003 Jun 15; 63(12):3370–3377. [Research Support, Non-U.S. Gov't Research Support, U.S. Gov't, P.H.S.]. [PubMed: 12810673]

47. Thurston G, Rudge JS, Ioffe E, Zhou H, Ross L, Croll SD, Glazer N, Holash J, McDonald DM, Yancopoulos GD. Angiopoietin-1 protects the adult vasculature against plasma leakage. Nat Med. 2000 Apr; 6(4):460–463. [Research Support, U.S. Gov't, P.H.S.]. [PubMed: 10742156]

48. Tian S, Hayes AJ, Metheny-Barlow LJ, Li LY. Stabilization of breast cancer xenograft tumour neovasculature by angiopoietin-1. Br J Cancer. 2002 Feb 12; 86(4):645–6551. [Research Support, U.S. Gov't, Non-P.H.S.]. [PubMed: 11870550]

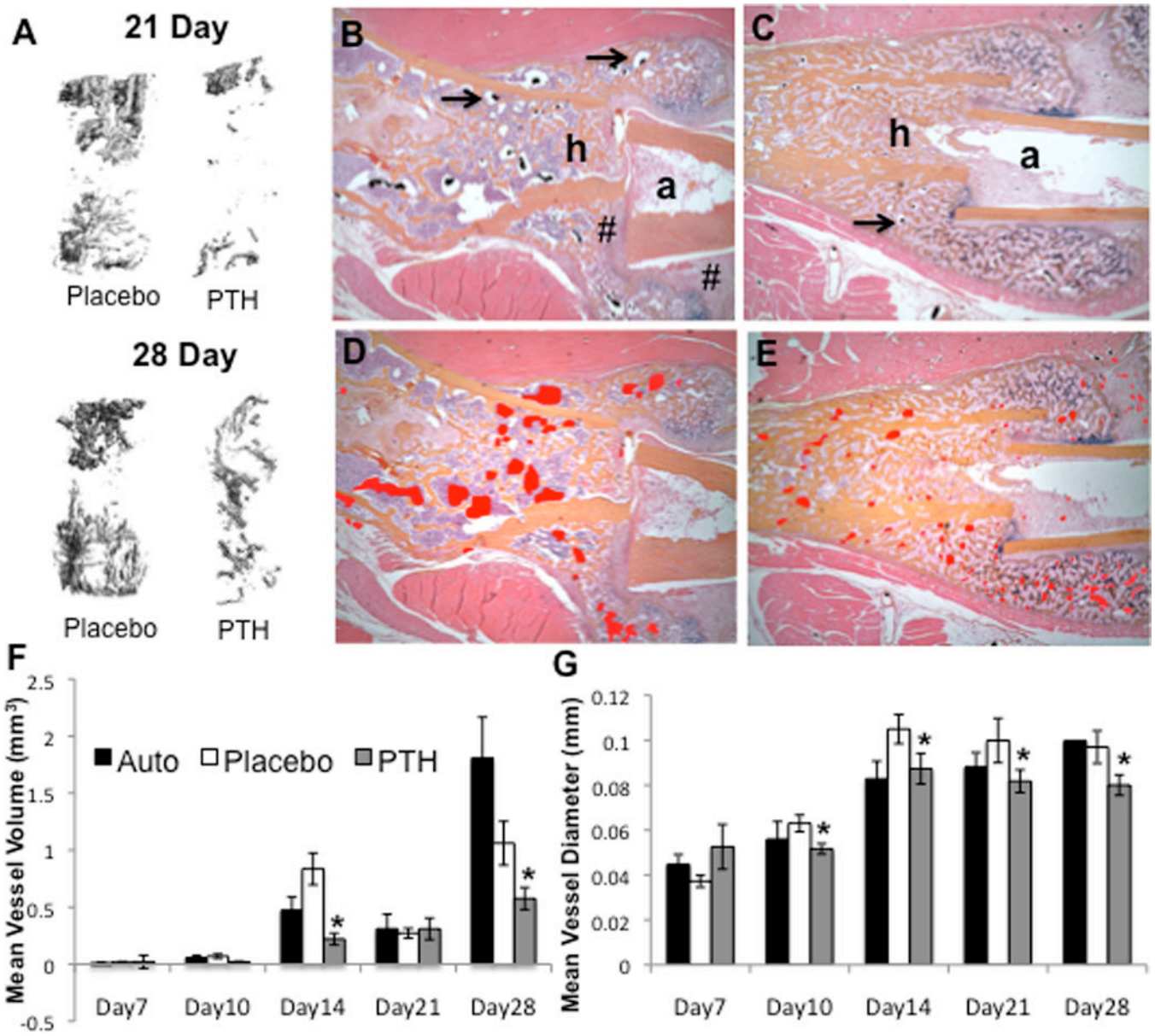

Figure 1. Intermittent PTH therapy alters vascularity of healing allografts

C57BL6 mice (n=5) received a femoral autograft or allograft surgery, and the allografted mice were randomized to daily Placebo (saline) or PTH (teriparatide) until they were euthanized via MICROFIL perfusion for vascular micro-CT analyses and subsequent decalcified histology. (**A**) Representative 3D reconstructions of the vascular contrast in the region of interest (ROI) of the allografts are shown to illustrate the difference in vascularity between the Placebo vs. PTH treatment on days 21 and 28. Representative micrographs (5× magnification) of orange G/alcian blue stained histology sections of the host (h) and allograft (a) junction of Placebo (**B**) and PTH (**C**) treated femurs isolated on day 21 are shown (arrows indicted the lead-chromate filled blood vessels). # indicates fibrotic tissue between host and allograft. To better illustrate the dramatic difference in the vascularity, the perfused vessel area is highlighted (red shaded regions in **D** & **E**). (**F,G**) Computed morphometry of the micro-CT data was performed to quantify the vascularity at the indicated time, and the data are presented as the mean +/− SD (*p<0.05 vs. Placebo).

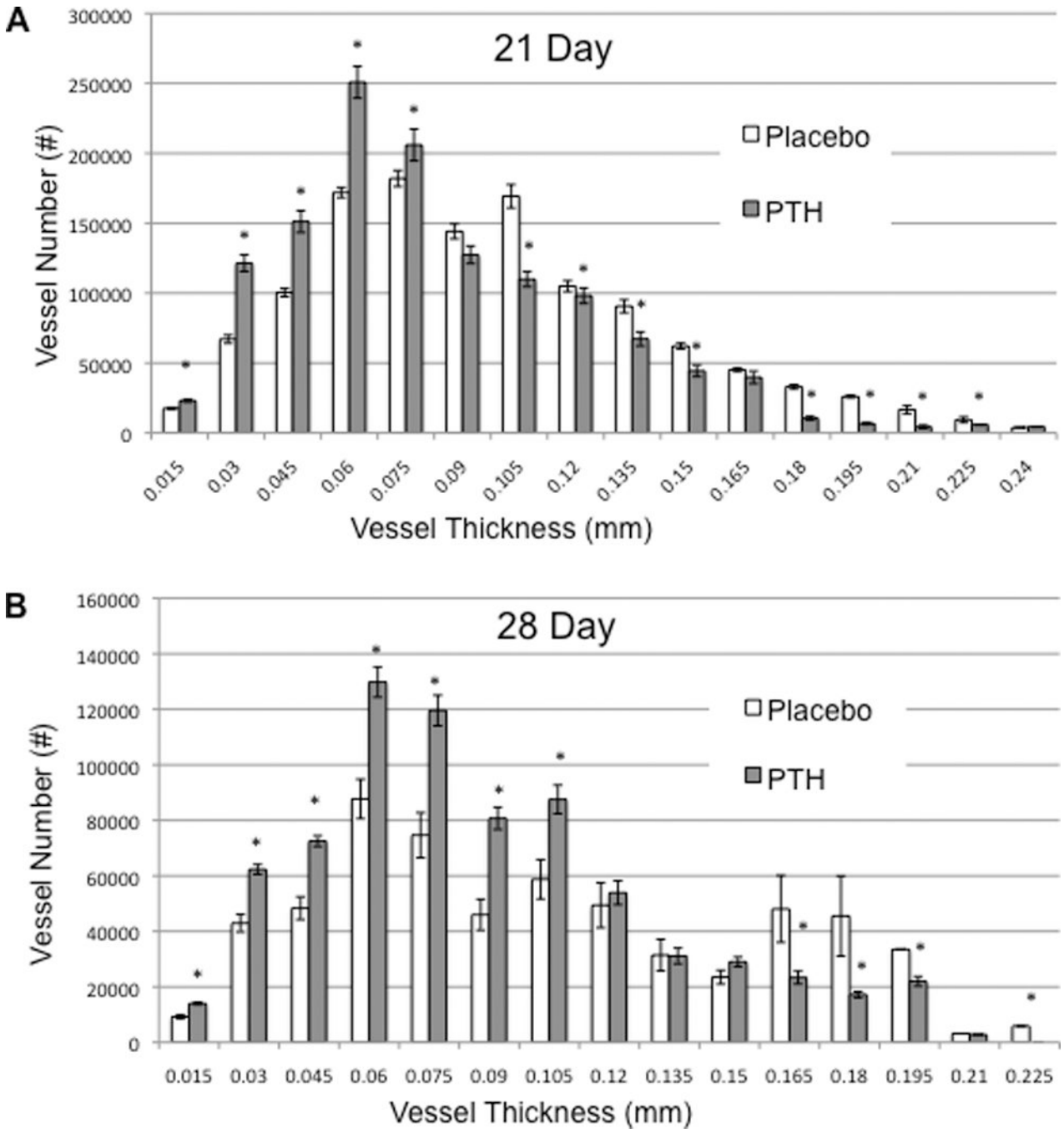

Figure 2. Intermittent PTH therapy during allograft healing increases small vessel angiogenesis while inhibiting large vessel arteriogenesis

The micro-CT data of the femoral allografts described in Figure 1 were further analyzed by binning the perfused vessels based on their diameter. The number of vessels per vessel size within the ROI of the allografts in Placebo and PTH treated mice on Day 21 (**A**) and Day 28 (**B**) are presented as the mean +/− SD (*$p<0.05$ vs. Placebo for the same vessel thickness).

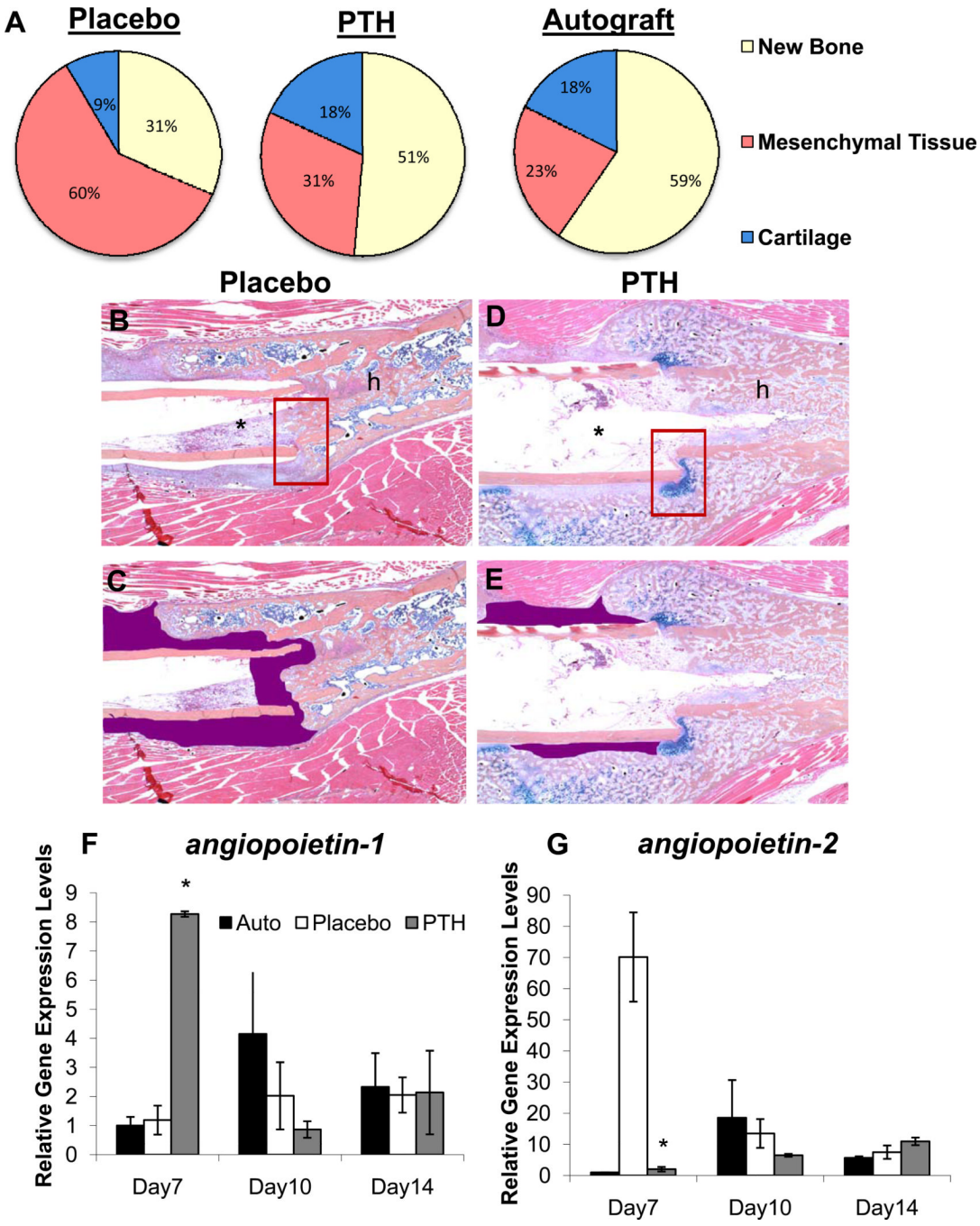

Figure 3. Intermittent PTH therapy significantly increases bone and cartilage formation while decreasing fibrosis with a significant increase in *angiopoietin-1*and down-regulation of *angiopoietin-2* expression during allograft healing

(**A**) Pilot histomorphometry data was collected from the Day 21 histology sections described in Figure 1 and the % area of new bone, undifferentiated mesenchymal tissue (fibrosis) and cartilage tissues within the ROI of the healing allografts was determined as the mean for each group (n=5). Representative orange G/alcian blue stained histology of placebo (**B** & **C**) and PTH (**D** & **E**) treated allografts are shown at 5× magnification in which the fibrotic tissue between the allograft (*) and the host (h) bone is highlighted (purple). Also note the fibrotic tissue in the placebo versus the alcian blue stained cartilage in the PTH treatment

that bridges the allograft-host junction (boxed region in **B** & **D**). Autografted and allografted femurs in wild type (C57BL/6) mice treated with Placebo or PTH were harvested on the indicated day and total RNA was extracted for qRT-PCR with primers specific for *angiopoietin-1* (**F**) and *angiopoietin-2*(**G**). The data are presented as the mean (n=5) +/− SD normalized to beta-actin control, where Autograft on Day 7=1 (*$p<0.05$ vs. Day 7 Placebo).

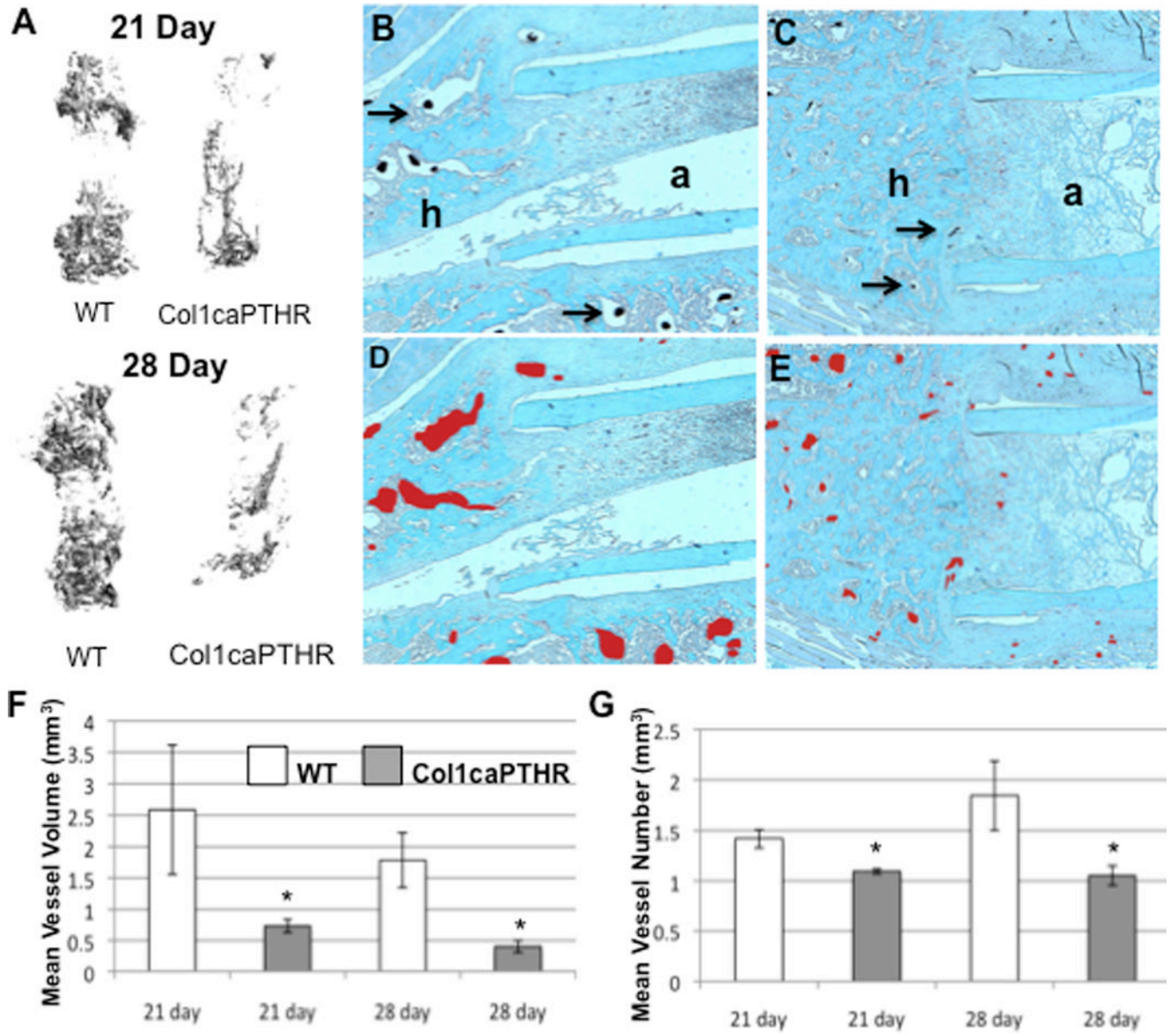

Figure 4. Constitutive PTHR signaling in osteoblasts decreases vascularity of healing allografts

Wild type (WT) C57B6 mice and their Col1caPTHR transgenic littermates (n=5) received a femoral allograft surgery, and were euthanized on day 21 or 28 via MICROFIL perfusion. Then the grafted femurs were harvested for vascular micro-CT and subsequent decalcified histology. (**A**) Representative 3D reconstructions of the vascular contrast in the ROI of the allografts are shown to illustrate the difference in vascularity between the WT vs. Col1caPTHR femurs on days 21 and 28. Representative micrographs (5× magnification) of safranin-O stained histology sections of the host (h) and allograft (a) junction of WT (**B**) and Col1caPTHR (**C**) allografted femurs isolated on day 21 are shown (arrows indicted the lead-chromate filled blood vessels). To better illustrate the difference in the vascularity, the perfused vessel area is highlighted (red shaded regions in **D** & **E**). (**F,G**) Computed morphometry analysis of the ROI was performed to quantify the vascularity at the indicated time (data are presented as the mean +/− SD (*p<0.05 vs. WT).

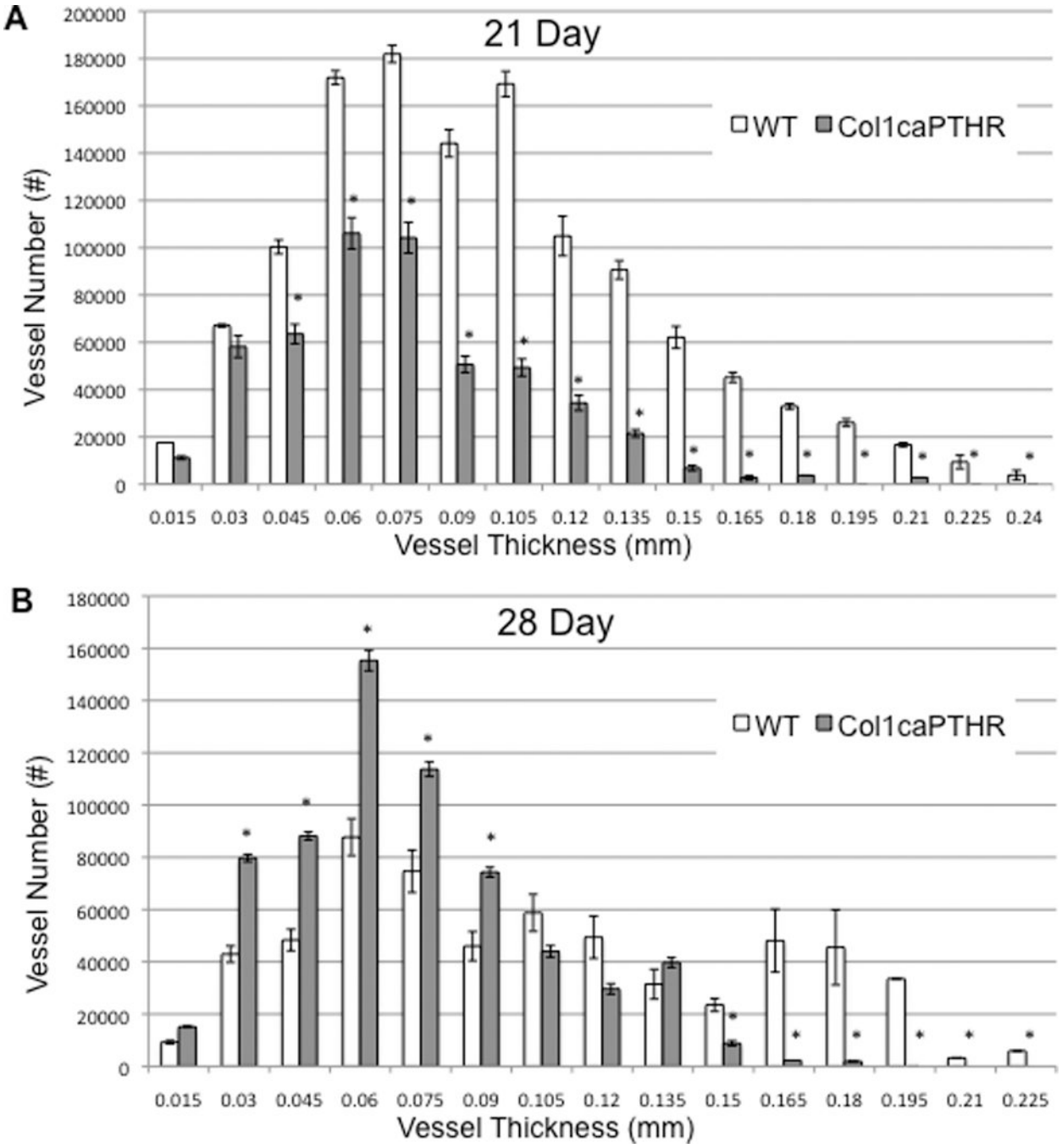

Figure 5. Constitutive PTH signaling in osteoblastic cells suppresses large vessel arteriogenesis throughout allograft healing, and stimulates delayed small vessel angiogenesis

The micro-CT data of the femoral allografts described in Figure 4 were further analyzed by binning the perfused vessels based on their diameter. The number of vessels per vessel size within the ROI of the allografts in WT (C57BL/6) and Col1caPTHR mice on Day 21 (**A**) and Day 28 (**B**) are presented as the mean +/− SD (*$p<0.05$ vs. WT for the same vessel thickness).

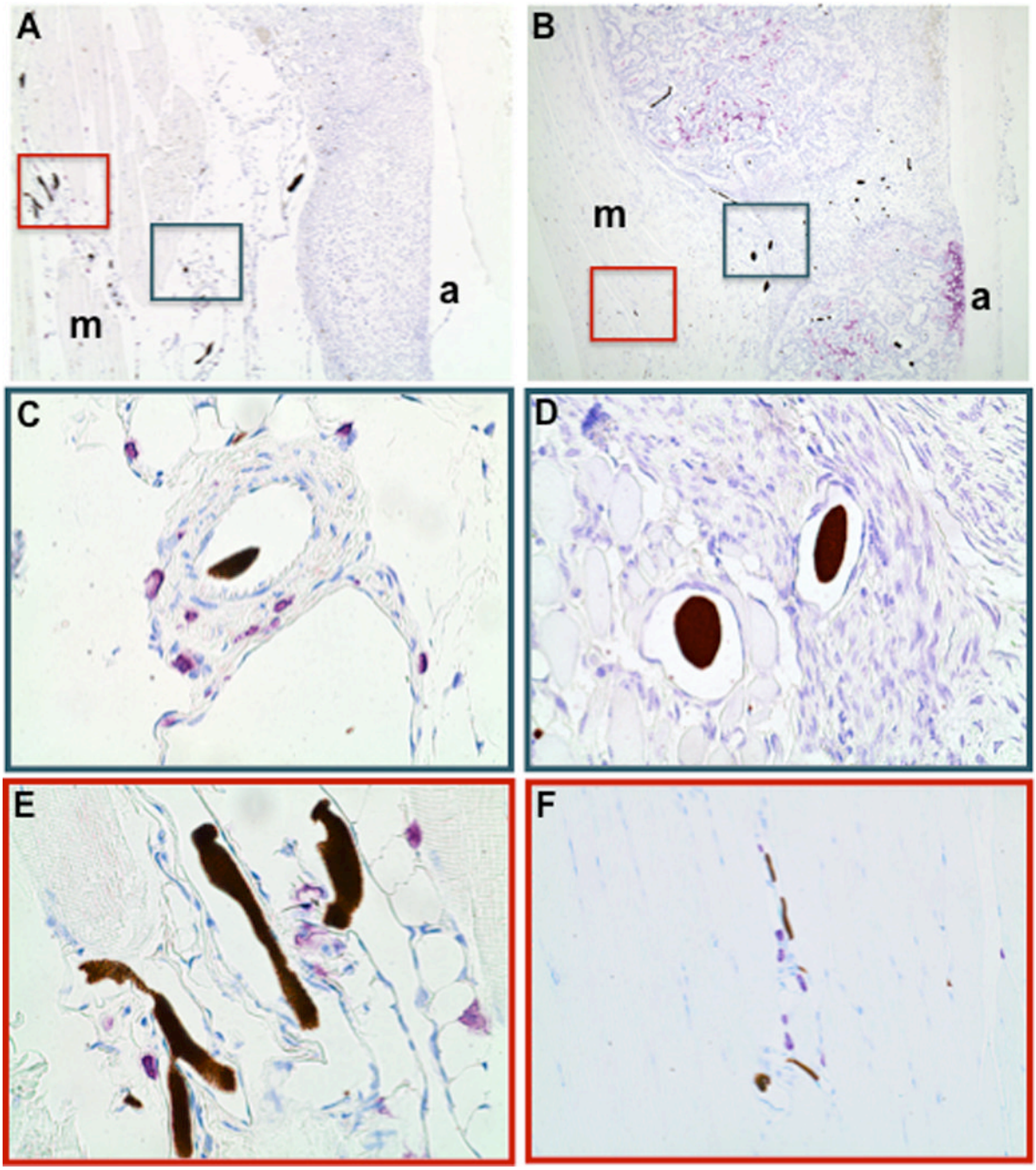

Figure 6. Intermittent PTH therapy decreases mast cell numbers in transitional tissue around healing allografts

Toluidine blue stained histology to identify mast cells was prepared from the femoral allografts described in Figure 1. Representative low power (5×) micrographs of the ROI including the allograft (a) and muscle (m) tissue interface of Placebo (A) and PTH (B) treated mice are shown. High power (40×) micrographs of the highlighted regions in A and B are shown to illustrate mast cell numbers (purple cells) and their proximity to lead-chromate perfused vessels in the transitional tissue (C and D) and adjacent muscle tissue (E and F) of healing allografts on Day 21.

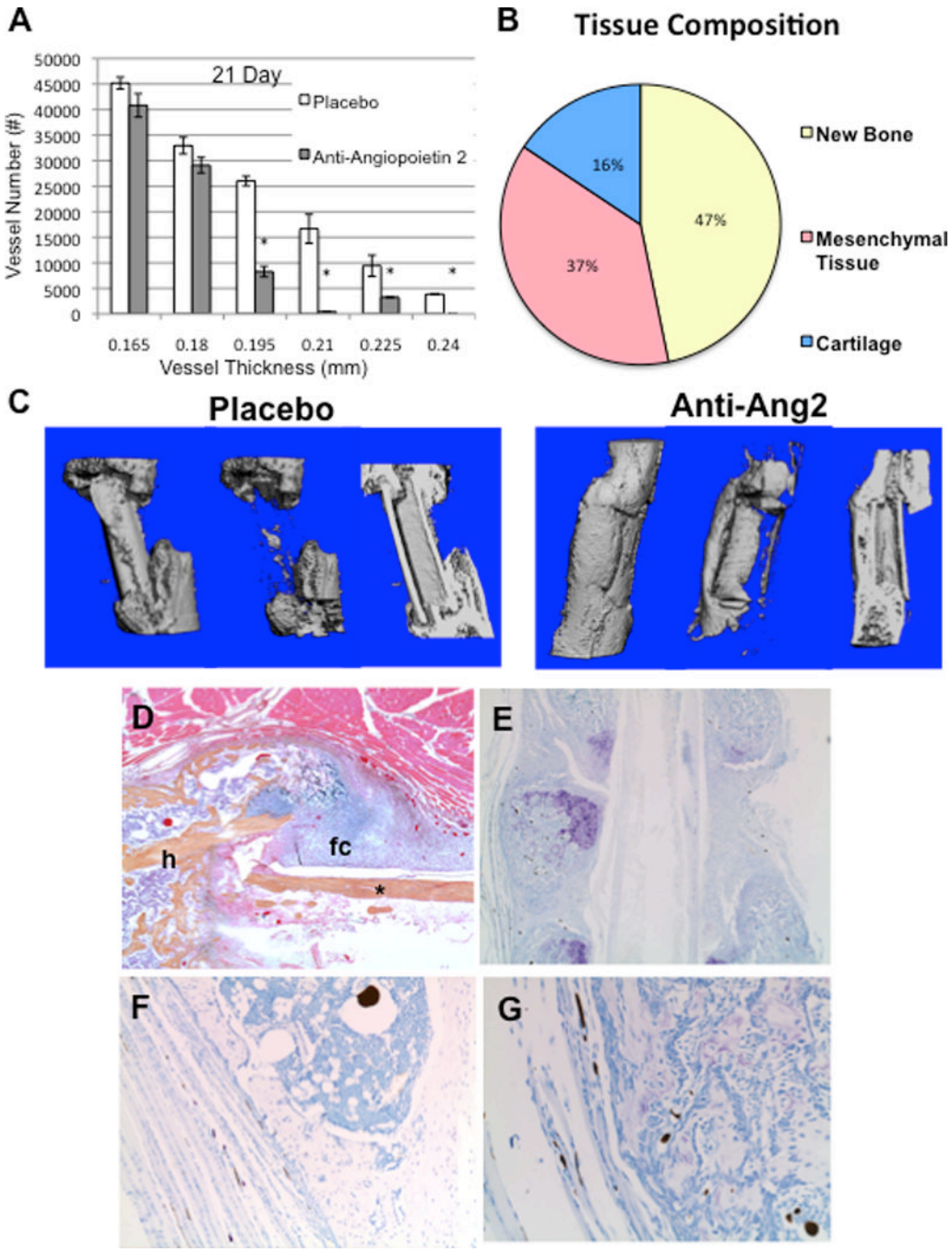

Figure 7. Anti-angiopoietin-2 (L1-10) treatment inhibits large vessel arteriogenesis, decreases fibrosis, mast cells and increases boney union during allograft healing

C57BL6 mice (n=5) received a femoral allograft surgery and were randomized to placebo or bi-weekly anti-angiopoietin-2 peptibody (L 1-10) therapy until they were euthanized on day 21. (**A**) Vascular micro-CT analyses were performed as described in Figure 2, and the data are presented as the mean +/− SD (*p<0.05 vs. placebo for the same vessel thickness). (**B**) Pilot histomorphometry data were collected as described in Figure 3a on the described allografted femurs. (**C**) Representative 3D reconstructions of the micro-CT scans of the total bone volume (left), callus bone volume (middle), and cross-section (right) of the allografts harvested from placebo and anti-angiopoietin-2 (L1-10) treated mice are shown to illustrate

the remarkable difference in host-to-host bridging new bone along the allograft. A representative low power (5×) micrograph of an H&E/Orange G stained section of the ROI including the allograft (*) and host (h) tissue interface from the anti-angiopoietin-2 treatment group is shown (**D**). Note the fibrocartilage (fc) that formed on the surface of the allograft at day 21. Micrographs of representative toluidine blue stained histology taken at 1.25× (**E**), and high power (20×) images (**F** & **G**) illustrated the lack of fibrosis, mast cells and perfused large vessels.

Table 1

Vascular Histomorphometry of Allografts at 21 days of Healing

Parameters	*Placebo*	*PTH*
Region of Interest (ROI) Area (mm^2)	13.85 ± 3.72	18.55 ± 0.93
Vessel Count	74 ± 30	137 ± 39 *
Vascular Area (mm^2)	0.32 ± 0.12	0.46 ± 0.12 *
Vascular Surface (mm)	17.17 ± 4.99	30.12 ± 7.84 *
Vascular Count per ROI Area	5.41 ± 2.25	7.44 ± 2.17 *
Vascular Surface per ROI Area	1.28 ± 0.41	1.63 ± 0.42 *

Pilot (n=5) histomorphometry was performed on the histology described in Figure 1 in which the 6mm mid diaphyseal area of the allografted femurs were used as the ROI (4mm of graft + 1mm of host at both proximal and distal graft-host junctions). The data are presented as the mean ± SD

* $p<0.05$ vs. Placebo.

Table 2

Histomorphometry of allografts into a Col1caPTHR and WT host mice at 21 days of healing

Parameters	*WT*	*Col1caPTHR*
Region of interest area (mm^2)	6.80±0.89	5.362±0.75
Host bone area (mm^2)	2.11±1.07	2.41±0.68
Graft bone area (mm^2)	0.78±0.08	0.53±0.20 *
Osteoclast number/graft area (mm^2)	5.53±3.08	9.09±5.49 *
Osteoclast surface/graft surface (%)	22.13±12.31	36.37±21.97 *

Pilot (n=5) histomorphometry was performed on the histology described in Figure 3 in which the 6mm mid diaphyseal area of the allografted femurs were used as the ROI (4mm of graft + 1mm of host at both proximal and distal graft-host junctions). The data are presented as the mean ± SD

* $p<0.05$ vs. WT.

Table 3

Mast Cell Histomorphometry of Allografts at 21 days of Healing

Parameters	*Placebo*	*PTH*
Region of Interest (ROI) Area (mm^2)	76.87 ± 17.44	70.97 ± 20.98
Total Mast Cell Count	170 ± 14	122 ± 17 *
Mast Cell /ROI Area (mm^2)	2.22 ± 0.07	1.72 ± 0.21 *
Mast Cells at Graft Host Junction	33 ± 9	14 ± 5 *

Pilot (n=5) histomorphometry was performed on the histology described in Figure 6 in which the 6mm mid diaphyseal area of the allografted femurs were used as the ROI (4mm of graft + 1mm of host at both proximal and distal graft-host junctions). The data are presented as the mean ± SD

* $p<0.05$ vs. Placebo.